Wetting of the adhesive fluid controls underwater adhesion in insects

Pranav Sudersan,[†] Michael Kappl,[†] Bat-El Pinchasik,[‡] Hans-Jürgen Butt,[†] and Thomas Endlein[*,†]

[†]*Max Planck Institute for Polymer Research, Ackermannweg 10, 55128 Mainz, Germany*

[‡]*School of Mechanical Engineering, Tel Aviv University, Tel Aviv-Yafo, Israel*

E-mail: endlein01@mpip-mainz.mpg.de

Abstract

Many insects can climb smooth surfaces using hairy adhesive pads on their legs. It was previously shown that a terrestrial beetle can even adhere and walk underwater. The naturally hydrophobic hairs trap an air bubble around the pads, allowing the hairs to make contact to the substrate like in air. However, it remained unclear to what extent such an air bubble is necessary for underwater adhesion. To investigate the role of the bubble, we measured the adhesive forces in individual legs of live but constrained ladybug beetles underwater in the presence and absence of a trapped bubble and compared it with its adhesion in air. Our experiments revealed that on a hydrophobic substrate, even without a bubble, the pads show adhesion comparable to that in air. On a hydrophilic substrate, underwater adhesion is significantly reduced, with or without a trapped bubble. We modelled the adhesion of a hairy pad using capillary forces. Coherent with our experiments, the model demonstrates that the wetting properties of the adhesive fluid secretion alone can determine the insects' adhesion in both air and underwater conditions and that an air bubble is not a prerequisite for their underwater adhesion.

1 Introduction

The question on how insects and other small arboreal animals climb smooth and slippery surfaces has fascinated scientists for the past three centuries[1,2]. We now know that such animals are able to adhere by using specialised organs on their feet called adhesive pads. These adhesive pads can generally be described as either "smooth" or "hairy". Several insect orders including earwigs, flies, and beetles[3] but also several spiders[4] and arboreal lizards[5] bear hairy pads. Hairy pads show 1) compliance to rough surfaces due to their lower effective modulus, 2) angle dependent adhesion due to asymmetric hair geometry and 3) self-cleaning capability[6], which makes them suitable to adhere to most surfaces reversibly. The hairs themselves (setae) can branch into smaller fibrillar units (spatulae) as seen in spiders and lizards but are typically undivided in most insects. The hairs in many insects can however exhibit different tip geometries, including discoidal, spatula shaped or pointed tips, and distributed throughout the pad depending on sex or species[7]. Single seta force measurements revealed that discoidal shaped seta show larger pull-off forces than spatula shaped or pointed setae[8], illustrating the role of hair geometry in adhesion. All insect pads secrete an adhesive fluid ("wet adhesion") while spiders and geckos rely on their dry hairy pads for attachment ("dry adhesion"). In the "wet adhesion" case, fluid secretion can enforce adhesion through surface tension and viscous forces[9], while, "dry adhesion" relies mostly on van der Waals forces[10].

While most of the studies on insect adhesion focused on terrestrial species, underwater insect attachment is much more rare and has been relatively unexplored. Some aquatic insects like diving beetles[11] or midge larva[12] use suction cups to adhere to surfaces. However, underwater adhesion using secreted liquids (glue-like substances or the adhesive fluid) requires the displacement of the water at the interface first and a spreading of the fluid on the substrate. One relatively simple approach is to use an air bubble around the adhesive organs similar to the air bubbles many secondary aquatic insects and spiders carry on their body for breathing underwater[13]. This has been shown in a recent study by Hosoda and Gorb[14]

that a terrestrial leaf beetle can attach quite well to surfaces underwater by using such an air bubble. Their naturally hydrophobic hairs trap the bubble around the pads when being submerged, which de-wets the surface effectively on contact. It has been hypothesised that a combination of capillary forces due the air bubble and hair secretions within the de-wetted area results in its adhesion underwater. However, it remained unclear whether an air bubble is strictly necessary and its exact contribution to the adhesive force. The oily adhesive fluid found in insects alone might be sufficient in creating the necessary capillary adhesion even without a bubble, given that the fluid remains on the hairs when submerged. In beetles, the tip of each seta secretes approximately one femtoliter of adhesive fluid[15]. The fluid's chemical composition was identified to be an oil-like mixture of mostly long chain hydrocarbons[16] with traces of triglycerides, fatty acids and cholesterol[17,18], rendering it immiscible with water.

The goal of this paper is to provide a generalised picture of adhesion in insects which use hairy pads and secrete an oily fluid for attachment. We used the ladybug beetle (*Coccinella septempunctata*) as an animal model to first experimentally measure adhesion force of its individual pads in air and underwater conditions, both on smooth hydrophilic and hydrophobic glass surfaces. We further tested whether the chemical profile of the adhesive fluid changes when the hairs were submerged in water. Second, we developed a simple theoretical model considering capillary forces to predict the net adhesion force of a hairy pad under different conditions. The case of underwater adhesion was studied both in the presence and absence of a trapped bubble, to decouple the bubble's role in the insect's adhesion. Finally, we discuss key insights gained from our experiments and model with regards to understanding adhesion in other animals.

2 Experimental

Normal adhesion force measurements on a restrained leg in a live beetle were performed. We characterised adhesion by the pull-off force during detachment, tested on smooth glass and fluorinated surfaces representing hydrophilic and hydrophobic substrates respectively. When no water was present, we labelled the contact type as "*in air*". Underwater, measurements were done both in the presence and absence of a trapped bubble ("*underwater: bubble*" and "*underwater: no bubble*", respectively) to investigate the bubble's role in underwater adhesion. Adhesion force for each of the labelled contact types were compared for both substrates.

2.1 Material and Methods

2.1.1 Insect preparation

Seven-spotted male adult ladybug beetles (*Coccinella septempuctata*) were purchased from Katz Biotech (Baruth, Germany) and housed in a plastic box filled with leaves, twigs and stones at room temperature and 60-80% relative humidity with daily access to sunlight. They were fed with raisins, honey and water *ad libitum*.

An individual beetle was first carefully anaesthetised using small amounts of CO_2 subliming from a piece of dry ice and then glued with a small dollop of epoxy glue on its elytra to the underside of a heavy steel ball. The ball was held in a bracket which allowed free rotational movement of the ball in each direction, thus helping to align the suspended beetle over the substrate (see Fig. 1). The bracket with the ball and the beetle could be further positioned by manual micro-manipulators in all three axes before the experiments. One front left leg was carefully fixed to a piece of soft solder wire coming off the steel ball using Blu Tack (Bostik Ltd., U.K.) allowing us to further align the leg to the substrate. The claws on the leg were also fixed to the wire using epoxy glue to prevent any further wiggling and to prevent the claws from touching the substrate. Each leg of a male ladybug beetle has two

pads. For the test, we only allowed the distal pad to come into contact with the substrate thus minimising partial or bad contact of the other one. A small piece of non-sticky Teflon tape helped to keep other legs tucked close to the body and avoided any interference during the adhesion test. After the measurements, the beetle was freed by carefully removing the epoxy glue and Blu Tack without harming it and set free.

2.1.2 Adhesion test

Adhesion measurements were performed on a custom force measurement setup developed in-house (Figure 1). A fibre optic displacement sensor (*Philtec D20, PHILTEC, Inc. USA*) together with a steel bending beam (spring constant = 68.1 N/m) constitutes the vertical force sensor. Beam deflection was calibrated using 4 different known weights to get the corresponding force. A plastic 3D printed substrate holder was glued to the end of the bending beam. The holder was designed to enable switching from one substrate to another without removing any glue. It also had transparent side walls which allowed us to fill it with water for the underwater experiments as well as observe the contact. The sensor was mounted on a stage consisting of a X-piezo element, used for precise lateral movements, XYZ motors, for coarse movements and a goniometer, for adjusting substrate alignment with the optics. Additionally, a separate Z-piezo element, fixed upright, was used for vertical up-down motion, bringing the insect in contact with the substrate from the top. A coaxial illuminated tube microscope (*Navitar*) with 2× objective and a stereo-microscope with 1× objective (*Wild Heerbrugg*) fit with digital video cameras (*FLIR Blackfly S*, 2448 x 2048 px; *Basler ace U*, 1280 x 1024 px) were used to record the sample contact with the substrate from ventral and side views respectively. Pad contact area was visualised through the substrate under reflection mode with the help of epi-illumination. The data acquisition from the force sensor and cameras, together with the appropriate piezo motion steps were synchronised using a custom LABVIEW program. Force data was acquired at a sample rate of 984 Hz, averaged to 512 points per motion step. Videos were recorded at 20 frames per second.

The vertical and lateral piezos were used together to perform approach-retract adhesion tests with the substrate to get the pull-off force. However, instead of a simple down-up motion, an additional 100 µm lateral sliding motion was introduced after the leg made contact, to ensure most of the hair tips align well with the substrate[7]. A further 10 µm compression step (approach) set all hairs in slight compression which helped further contact with the surface. Next, a short pause (1 s) removed any viscoelastic effects before finally retracting the leg away from the substrate. All approach, retract and lateral slide motion was done at a speed of 62.5 µm/s. Ventral view video recordings were used for contact area extraction while the side view imaging was used to visually aid orienting the pad with the substrate before a test.

For underwater experiments, 1 ml Milli-Q water was pipetted into the substrate holder. In order to achieve an underwater contact without a trapped air bubble, the water was first degassed in a vacuum chamber at 10 mbar pressure for 3 hours and used immediately. Before the experiments, the pad was brought into contact with the surface 10 times repeatedly to equilibrate the pad's secretion system.

Five force measurements were subsequently performed on a fresh spot of the substrate and averaged for data analysis. Experiments were repeated with five individual beetles for each type of contact and substrate. In total, 30 beetles were tested.

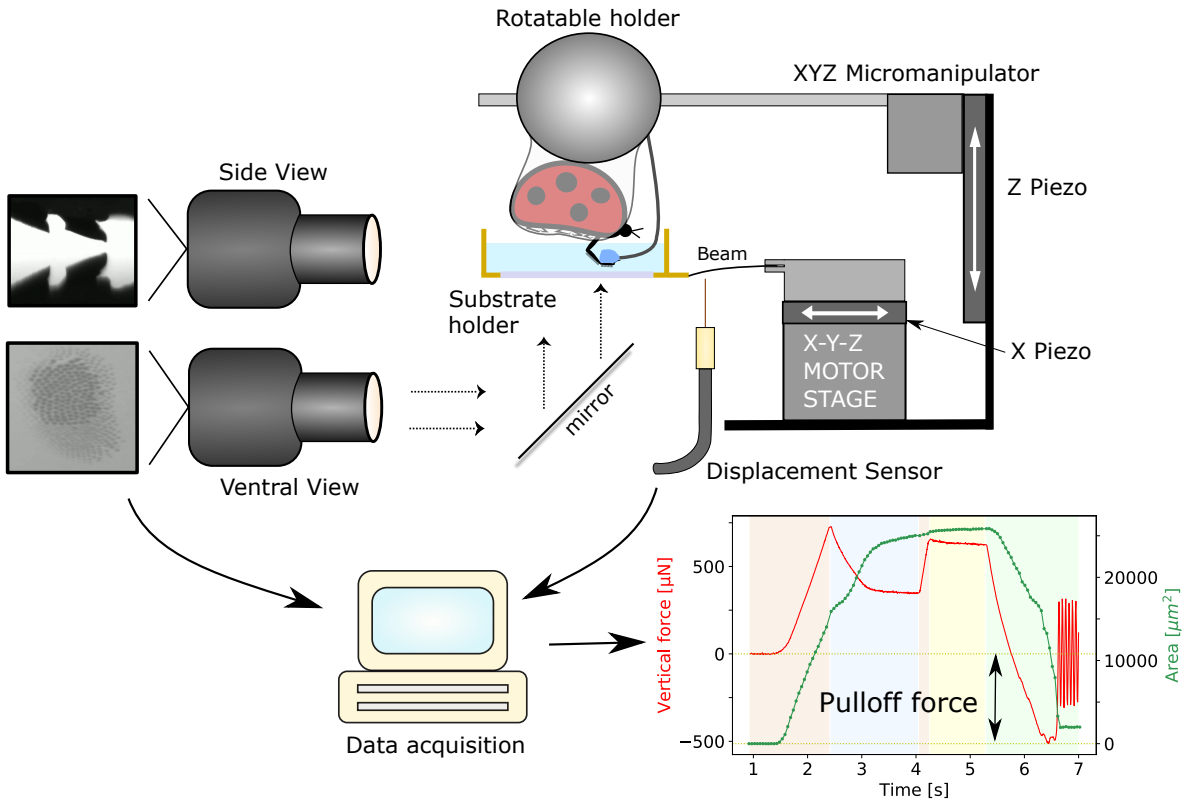

Figure 1: Adhesion setup (for explanation see text). The recorded force data and contact area of a distal pad are shown in the plot, in which, the shaded regions from left to right represent the distinct movement sequence: approach, lateral pull, approach, pause and retract, respectively. Negative force values represent attraction and the minimum force peak during the final retraction step is the adhesion force used for further analysis. An animated version of a typical force recording is available in the Supplementary Material.

2.1.3 Data analysis

Extraction of pull-off force from force data, image processing, plotting and statistical analysis were all performed in "*Buggee*", a tool written in Python using open-source libraries for synchronous analysis of force data and video recordings (`https://github.com/PranavSudersan/Buggee`).

For measurements in air, the pull-off force was defined as the minimum negative force during the final retraction step (Figure 1). For underwater measurements, an additional

correction was necessary. When the beetle was submerged underwater, its contact line at the water surface shifted, which influenced the force readout due to surface tension effects. This effect needed to be cancelled. So, a "background" force data was recorded, where the submerged beetle makes no contact with the substrate. This background data was then subtracted from a typical force data with substrate contact to correct for the external surface tension effects. The pull-off force was subsequently calculated from the minima as before.

Data sets were compared for statistical differences using pairwise Student t-test and their corresponding p-value and Common Language Effect Size (CLES) are reported. Shapiro-Wilk test was done for each data set to verify a normal distribution of its residuals and Levene's test was done to check for variance homogeneity, to validate the t-test assumptions. Bonferroni's correction was used to account for multiple comparison between groups.

2.1.4 Substrate preparation

Standard 20 mm wide glass cover-slips were used as the hydrophilic substrate. Glass was wiped with isopropanol, rinsed in water and dried under nitrogen flow. The surface was then plasma cleaned in a oxygen plasma chamber (Diener Electronic Femto) for 10 min at 120 W. The surface was further rinsed with water and dried under nitrogen flow.

For the hydrophobic substrate, the glass cover slip was coated with a fluorosilane via chemical vapour deposition (CVD). First, the glass was cleaned using IPA and plasma treated as before. Next, 0.2 ml of Trichloro(1H,1H,2H,2H-perfluorooctyl) silane (PFOTS), procured from Sigma Aldrich, was put in a sealed chamber along with the the cleaned glass. The chamber was placed under 100 mbar pressure for 10 min for the CVD process. Finally, the substrate was annealed at 150℃ for 3 hours.

The substrate wetting was characterised by dynamic contact angle measurements, performed with a DataPhysics OCA 35 contact angle goniometer. Milli-Q water and n-hexadecane were used as test liquids. Advancing and receding contact angles were measured for a maximum drop volume of 10 µl and with 0.5 µl/s flow rate.

Table 1: Dynamic contact angles measurements

Substrate	Liquid	θ_A	θ_R
Glass	Water	63±5°	20±2°
	n-Hexadecane	<10°	<10°
PFOTS	Water	122±1°	93±2°
	n-Hexadecane	88±2°	56±5°

2.1.5 Field desorption mass spectroscopy

A previous study on arachnids[19] reported that its secreted fluid does not dissolve in water. To test whether the beetles retain their adhesive fluid underwater unchanged, we performed a Field Desorption Mass Spectroscopy (FDMS) using a ZAB 2-SE-FPD spectrometer (VG Instruments). The measurements were done on the extracted secretions before and after rinsing its legs with water. The middle leg of an Asian ladybird (*Harmonia axyridis*) was immersed in 50 µL THF for 20 min and then transferred to the measurement chamber of the FDMS. As a reference, pure THF was used. The second middle leg of the same ladybird was subsequently immersed in 100 µL Milli-Q water for 15 min, then in THF for 20 min and then transferred to the measurement chamber of the spectrometer. Molecular composition was extracted from the peak positions of the FDMS spectra.

2.2 Results

2.2.1 Adhesion measurements

In air, adhesion forces of the distal pad of ladybug beetle against glass and PFOTS were similar, i.e. no significant differences were detected (Figure 2 and Table A.1). In contrast, the underwater adhesion on a PFOTS surface was significantly larger than on glass ($p < 0.001$). This stronger adhesion on PFOTS was observed both in the presence and absence of a trapped bubble. In both cases, the adhesion force reached similar values as in air. In contrast, on glass, adhesion underwater was significantly reduced when compared to dry conditions, irrespective of the presence of a trapped bubble ($p \leq 0.002$). In the presence of

a bubble, underwater adhesion on glass was slightly higher (CLES = 0.84, p = 0.07).

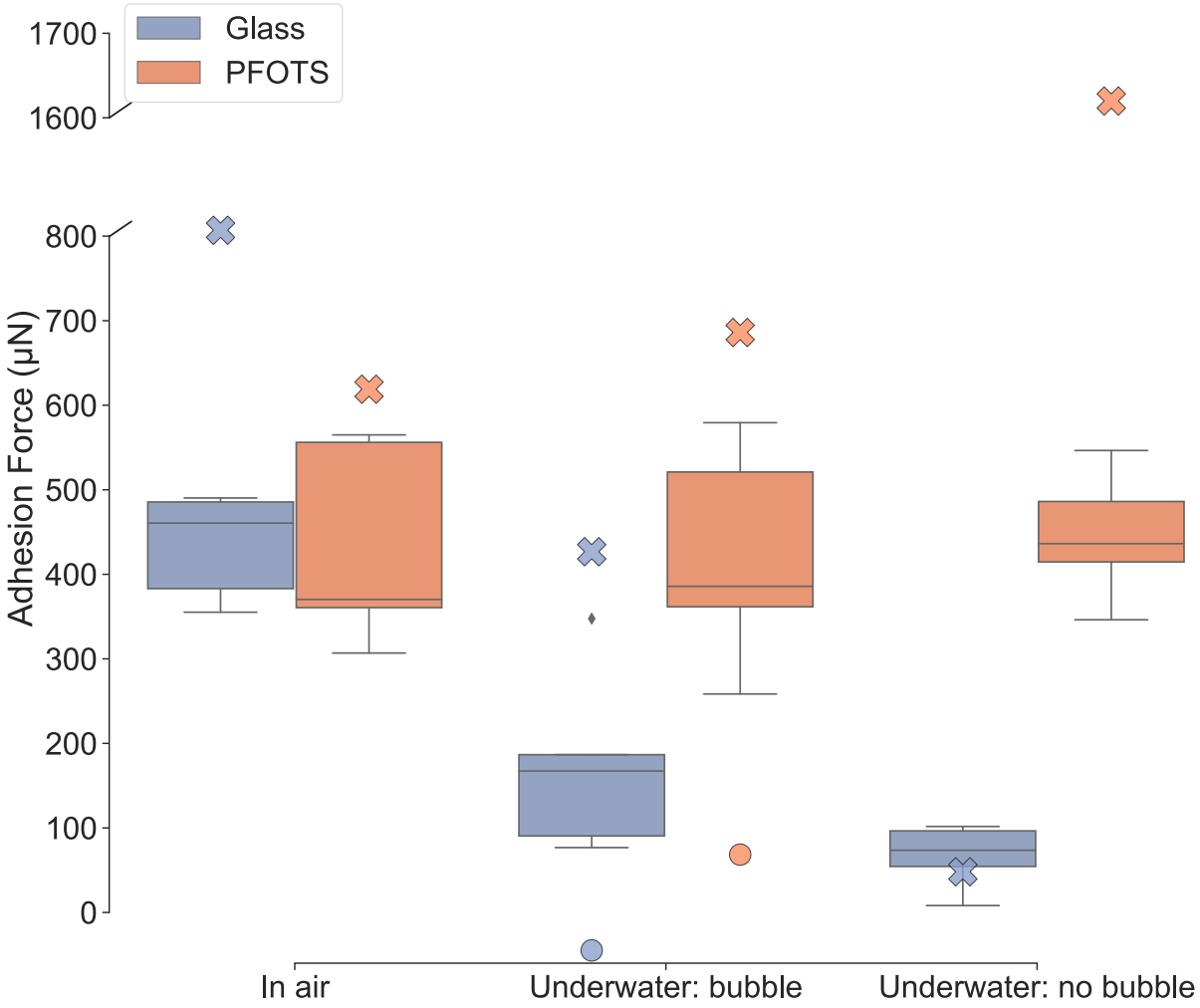

Figure 2: Box-and-whisker plot showing single leg adhesion force measurements of ladybug beetle (*Coccinella septempuctata*) on glass and PFOTS substrates in air and underwater conditions. The two types of contact during underwater experiments are represented separately: "*bubble*" and "*no bubble*". Crosses represent theoretical predictions of adhesion force, while, circles represent the contribution of the bubble itself, calculated from the capillary bridge model. In the model, hair diameter = 4 µm, pad diameter = 200 µm, hair height = 40 µm, N_{hairs} = 500, V_{fluid} = 4.2 fL and V_{bubble} = 1.2 nL. Interfacial tension of the adhesive fluid in air and water were assumed to be 24 mN/m and 48 mN/m respectively and water surface tension is 72 mN/m.

Apart from the three depicted contact types, we observed an additional fourth type which occurred in roughly 25% of our underwater experiments. In this scenario, the ventral view recordings show that the hairs did not appear to contact well with the substrate, unlike the

other three contact types. This "bad contact" scenario shows no adhesion with either glass or PFOTS substrate. While it was not completely clear why such a contact occurs, there can be two possible reasons. First, the hairs could get bundled due to a small air meniscus within the hairs, resulting in their disorientation. Second, a thin water layer at the substrate interface might not be drained out to allow the hairs to make contact with the substrate, resulting in a loss of adhesion.

2.2.2 Field desorption mass spectroscopy

FDMS results confirm the presence of adhesive fluid on an Asian ladybird's leg when underwater (Table 2). Molecular weights of the secreted fluid mixtures extracted from the beetle's leg, without and after immersion in water, show that, except for two molecular weights (406.8 g/mol and 331.6 g/mol), the chemical fingerprint remained unchanged This indicates that the adhesion fluid was not washed away underwater. Probable compounds in the fluid, corresponding to the resultant molecular weights, include mostly aliphatic hydrocarbons with traces of aldehydes. Our preliminary measurements on *Harmonia axyridis* gives us confidence to assert that, even for the case of *Coccinella septempuctata*, the adhesive fluid was not washed away from the hairs during the underwater experiments.

Table 2: Molecular weights of adhesive fluid secretion of *Harmonia axyridis* with and without rinsing the beetle's leg in water.

Without rinsing (g/mol)	After rinsing (g/mol)	Probable compounds
324.5	324.5	$C_{23}H_{48}$, $C_{22}H_{44}O$
	331.6	$C_{24}H_{44}$
350.5	350.5	$C_{25}H_{50}$
352.5	352.5	$C_{25}H_{52}$, $C_{24}H_{48}O$
378.5	378.5	$C_{27}H_{54}$
404.6	404.5	$C_{29}H_{56}$
406.8		$C_{29}H_{58}$
432.8	432.7	$C_{31}H_{60}$

3 Theory

3.1 Capillary Bridge Model

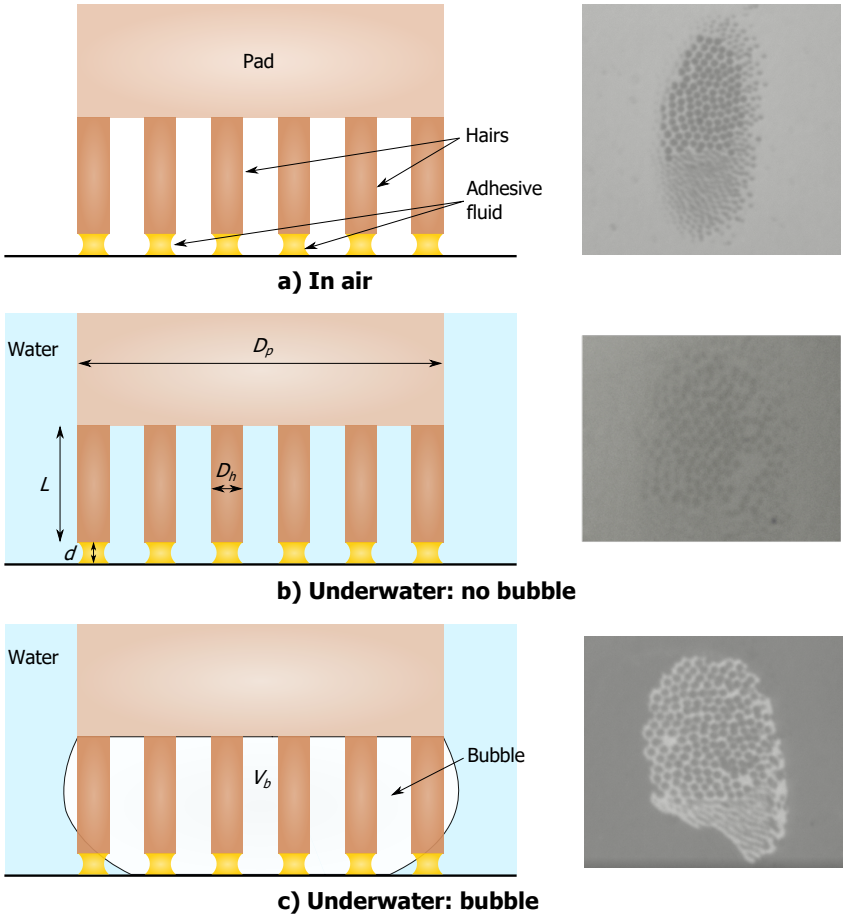

Figure 3: The capillary bridge model. The hairs make contact with the substrate in three ways: a) *In air*, where the adhesive fluid bridges are surrounded by air; b) *Underwater: no bubble*, where the adhesive fluid bridges are fully surrounded by water; c) *Underwater: bubble*, where part of the adhesive fluid bridges are inside the bubble while others are outside in water. The corresponding ventral view contact images of the beetle's pad are shown on the right.

We modelled the hairy pad as an array of N cylindrical rods of length, L, and diameter, D_h, fixed to a flat circular pad of diameter, D_p (Figure 3). The hairs and the pad were assumed to be perfectly rigid, for simplicity. The tip of each hair has an adhesive fluid of volume, V_f, making contact with the substrate. The fluid is pinned to the circumference of the hair and

forms a capillary bridge of height, d. Similar to our experiments, we considered three types of contacts for the pad: 1) *In air*, 2) *Underwater: no bubble* and 3) *Underwater: bubble*. In the third case, a bubble of volume, V_b, is trapped between the hairs and pinned to the pad circumference.

To characterise the adhesive fluid and bubble volume, we defined two radii, s_f and s_b, respectively, by $V_f = \frac{4}{3}\pi s_f^3$ and $V_b = \frac{4}{3}\pi s_b^3$. Here, s_f and s_b are the radii of spheres with equivalent volumes. Fluid and bubble radii were assumed to scale proportional to their corresponding pinned contact diameter. We thus defined the size parameters, $\phi_f = D_h/(2s_f)$ and $\phi_b = D_p/(2s_b)$ for the fluid and bubble respectively, to conveniently scale their volumes relative to the hair and pad diameters they are pinned to.

The net force for cases 1 and 2 can be calculated as:

$$F_{net} = Nf \tag{1}$$

Here, f is the capillary force of a single fluid bridge at a distance, d, in air (f_{air}) or underwater (f_{water}).

For case 3, the net force is given by:

$$F_{net} = N_{in}f_{air} + N_{out}f_{water} + f_{bubble} \tag{2}$$

Here, N_{in} and N_{out} are the number of hairs inside and outside the bubble, respectively, f_{air} and f_{water} are the capillary forces of the fluid bridge inside and outside the bubble, respectively, and f_{bubble} is the capillary force contribution due to the bubble meniscus alone at distance $d + L$.

The capillary force, f, is the sum of two contributions: surface tension and Laplace pressure (equation A.1). Force versus distance for a single capillary bridge was calculated by Surface Evolver simulations[20] (described in A.1), and used to obtain F_{net} as a function of d for each type of contact. The adhesion force of the complete hairy pad system was then

obtained from the minima of F_{net}, where negative force values represent attraction.

We considered f_{air} and f_{water} to be distinct terms because the capillary force by the adhesive fluid would be different in air and underwater due to its different contact angle and interfacial tension in each case. Using the Young-Duprè equations for each case of fluid-air, fluid-water and water-air interface, one can derive the following relation for the contact angle of the adhesive fluid underwater:

$$\cos\theta_{fw} = \frac{\gamma_{fa}\cos\theta_{fa} - \gamma_{wa}\cos\theta_{wa}}{\gamma_{fw}} \tag{3}$$

Here, θ_{fw} and θ_{fa} are the contact angles of the adhesive fluid with the substrate in water and air respectively, θ_{wa} is the contact angle of water with the substrate in air, γ_{fa} is the surface tension of the adhesive fluid, γ_{wa} is the surface tension of water and γ_{fw} is the interfacial tension of the adhesive fluid with water.

All lengths were normalised w.r.t. s_f and forces were normalized w.r.t. $\gamma_{fa}s_f$. Interfacial tension values were fixed relative to γ_{fa}. Non dimensional bubble volume was expressed as, $\hat{V_b} = V_b/s_f^3$

Geometric parameters and interfacial properties were kept fixed for all model calculations (Table 3). Here, we assumed the adhesive fluid to be an oil-lke substance and thus the interfacial tension ratios γ_{wa}/γ_{fa} and γ_{fw}/γ_{fa} were taken corresponding to typical values for oil and water. We considered representative hydrophilic and hydrophobic substrates with θ_{fa} and θ_{wa} values corresponding to a typical glass and fluorinated surface, respectively. Area fraction of the hairs relative to the pad, $\alpha = ND_h^2/D_p^2$, hair aspect ratio, L/D_h, and fluid size parameter, ϕ_f, were fixed to values typical for a ladybug's hairy pad.

First, we calculated force-distance curves for a single pinned liquid capillary bridge. Second, the effect of substrate on the force-distance curves of the hairy pad system was compared for each type of contact. Third, we looked at the effect of changing the bubble volume, $\hat{V_b}$, on the net underwater adhesion. Finally, the influence of varying the hair diameter, D_h, on adhesion was studied for each case.

Table 3: Fixed parameters of the capillary bridge model

Property	Value
Area fraction, α	0.1
Hair aspect ratio, L/D_h	10
Water surface tension ratio, γ_{wa}/γ_{fa}	3
Fluid-water interfacial tension ratio, γ_{fw}/γ_{fa}	2
Fluid size parameter, ϕ_f	2
Hydrophilic substrate	$\theta_{fa} = 6°$, $\theta_{wa} = 24°$
Hydrophobic substrate	$\theta_{fa} = 50°$, $\theta_{wa} = 120°$

3.2 Capillary force of a pinned liquid bridge

Forces due to a single pinned capillary liquid bridge in contact with a substrate were obtained via Surface Evolver simulations (Figure 4). We see that, generally, the shape of the liquid meniscus determines the strength of its adhesion force. High adhesion is seen for contact angles less than $\sim 70°$ due to a net negative curvature of the meniscus, while low adhesion is seen for contact angles greater than $\sim 150°$ due to its net curvature being close to zero. The Laplace pressure contribution to the net adhesion force dominates for contact angles less than 100° (Figure 4b). Interestingly, its contribution to the adhesion force is mostly non-repulsive for contact angles greater than 90°. This is because, the low volume of the liquid and its pinned contact line prevents the meniscus from having a high positive curvature due to geometric constraints. Only for a contact angle of 150°, the liquid's curvature becomes positive, manifested in its slightly repulsive Laplace contribution. Surface tension makes a significant contribution to the net force only for a small range of contact angles close to 90°. For contact angles greater than 150°, the net adhesion force approaches zero.

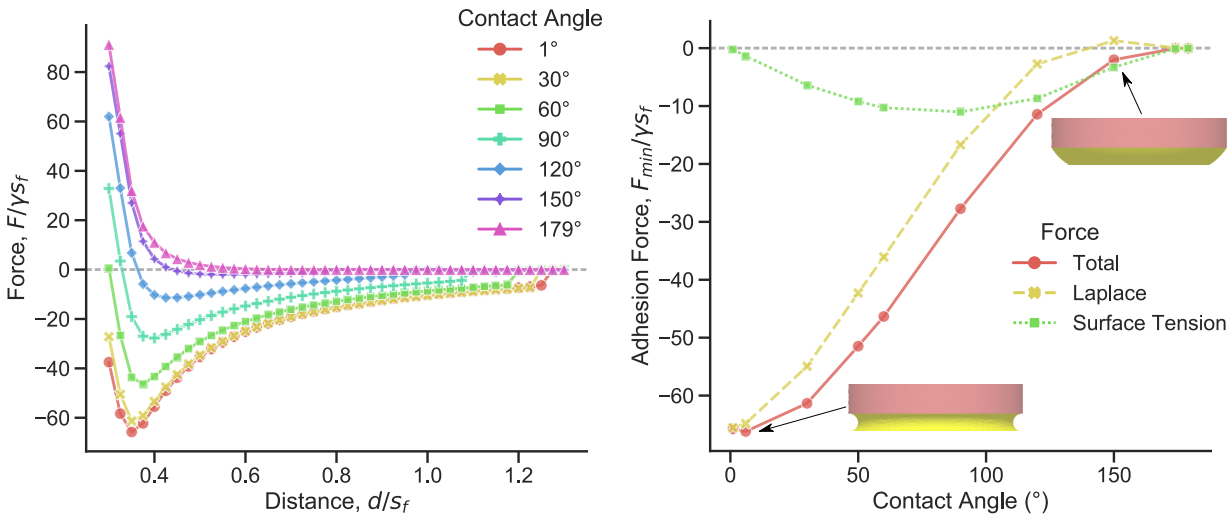

(a) Force-distance curves

(b) Force contributions

Figure 4: Normalised capillary force of a single liquid bridge in contact with a substrate and pinned to a circular perimeter on top. Fluid size parameter, $\phi_f = 2$. Negative force values represents attraction. a) Force-distance curves are shown for different contact angles of the liquid with the substrate. b) Adhesion forces, calculated from the minima of the corresponding force-distance curves, are plotted as a function of contact angle with the substrate, together with its Laplace and surface tension components (equation A.1). Simulation snapshots of the liquid meniscus corresponding to angles 6° and 150° are depicted.

The force-distance curves show a general trend of being repulsive at small distances (Figure 4a). This is a result of the pinned contact line on the top. A limited volume is available for the liquid to occupy when the gap distance is small, causing the meniscus shape to bulge outwards near the pinned contact line. This creates a net positive curvature, resulting in a positive Laplace pressure and thus repulsion. Without pinning, the capillary forces would have shown high attractive forces on a hydrophilic substrate[21].

3.3 Effect of the substrate

The normalised force-distance curves of a hairy pad system on a hydrophilic and hydrophobic substrate are predicted based on the capillary bridge model and compared for the different contact types (Figure 5). The forces in each case are calculated from equations (1) and (2) for fixed geometric and interfacial properties (Table 3).

On the hydrophilic substrate ($\theta_{wa} = 24°$), highest adhesion is seen when the hairs contact in air, while lowest adhesion occurs underwater without a trapped bubble. The presence of a bubble leads to intermediate force values. In contrast, on a hydrophobic substrate ($\theta_{wa} = 120°$), highest adhesion is seen for the underwater case without a trapped bubble, much larger than in air. When a bubble is present, the forces are only slightly larger than in air.

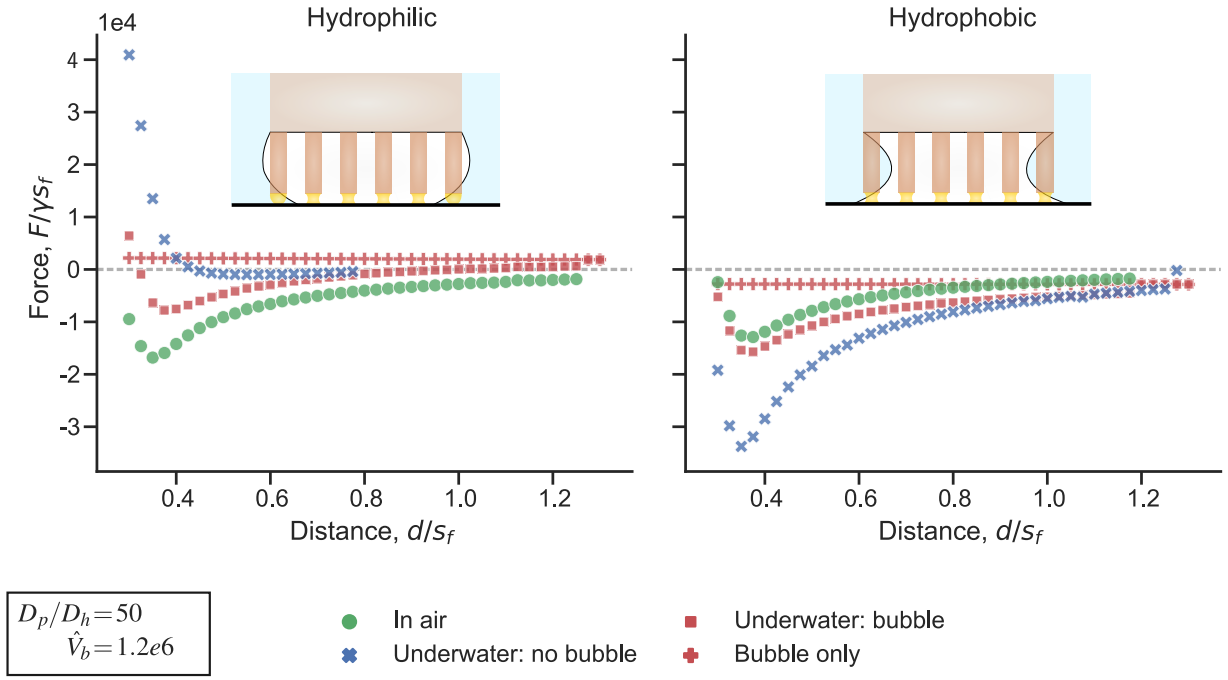

Figure 5: Theoretical force-distance curves of a hairy pad system on a hydrophilic and hydrophobic substrate in air and underwater conditions. A negative force value represents attraction. Normalised forces are calculated from the capillary bridge model, with model parameters listed in Table 3. The bubble's contribution to the net force for an *underwater: bubble* contact is denoted by plus symbols. Insets represent the *underwater: bubble* contact for each substrate.

The observed trend in forces can be explained by how the adhesive fluid wets the surface in each case. On a hydrophilic substrate, the contact angle of the oily adhesive fluid is 6°, when surrounded by air (Table 3) and 150°, when surrounded by water (equation (3)). This results in the meniscus shape to have a net negative and slightly positive curvatures, respectively, resulting in strong adhesion in air and poor adhesion underwater. On a hydrophobic

substrate however, the contact angles of the fluid in air and water are 50° and 1°, respectively. In both cases, the contact angles are low, resulting in strong adhesion in both media. Additionally, the interfacial tension of the oily fluid underwater (γ_{fw}) is twice that of in air (γ_{fa}). Thus, we see a higher capillary adhesion for the *underwater: no bubble* case when compared to *in air* (Figure 6). Note that the contact area is fixed in all cases by keeping the area fraction and D_p/D_h constant. Thus the observed effects is not a result of changing contact area, but rather on the nature of capillary forces.

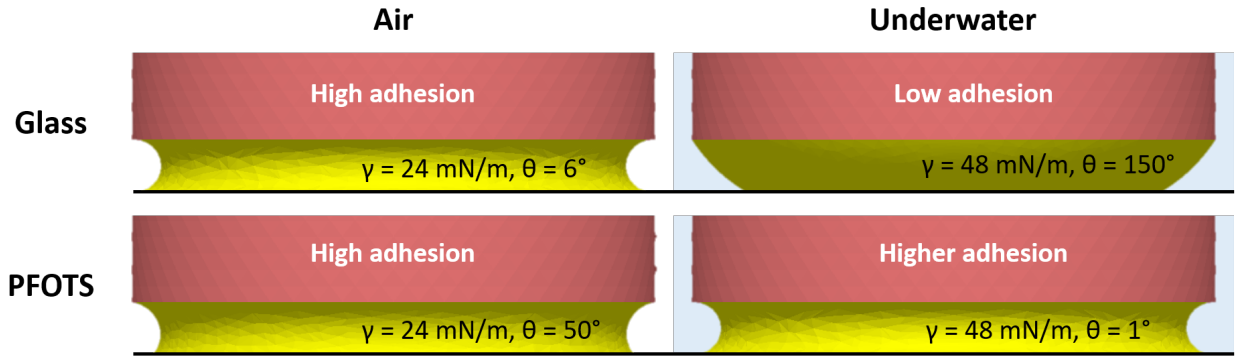

Figure 6: Simulation snapshots of oil capillary meniscus in contact with glass and PFOTS in air and underwater conditions. The corresponding interfacial tension, γ, and contact angle, θ, used to predict the ladybug's adhesion are labelled for each case.

The net force in the *underwater: bubble* case mainly depends on the proportion of hairs inside and outside the bubble (equation (2)). For the given bubble volume, only part of the hairs are inside the bubble for the hydrophilic substrate, while, all the hairs are inside the bubble for the hydrophobic substrate. Therefore, the force curve lies between *in air* and *underwater: no bubble* cases for a hydrophilic substrate, and closely follows the *in air* case for a hydrophobic substrate.

We observed that the bubble itself doesn't contribute much to the net force on either substrate (Figure 5). Its contribution even is slightly repulsive on the hydrophilic substrate due to the positive curvature of the bubble, and slightly attractive on the hydrophobic substrate due to its negative curvature. This small contribution is manifested by the slightly higher adhesion for *underwater: bubble* relative to *in air* for the hydrophobic substrate, since

all hairs are within the bubble in this case.

3.4 Effect of bubble volume

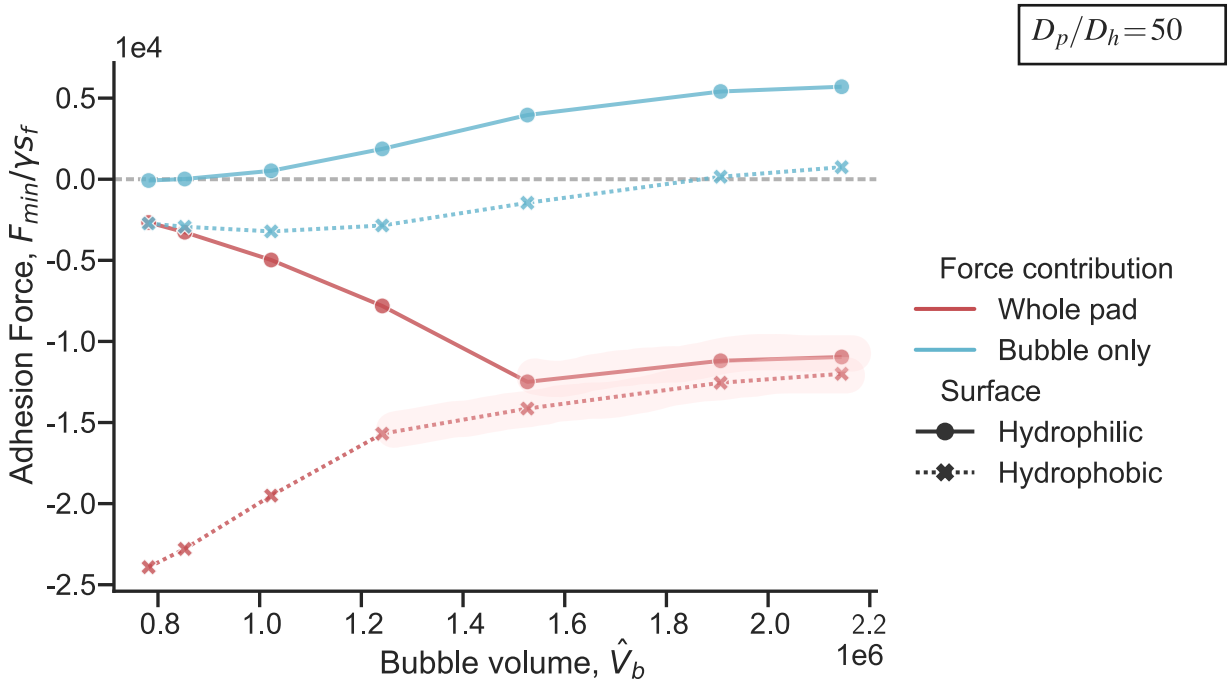

Figure 7: Normalised adhesion force of a hairy pad system as a function of bubble volume, $\hat{V}_b$, for the *underwater: bubble* contact type. Adhesion forces are calculated from the minima of the respective force-distance curves. Negative force value represents attraction. Pad to hair diameter ratio (D_p/D_h) is kept fixed. Highlighted regions represent entrapment of all hairs within the bubble.

The volume of the bubble can influence its capillary force contribution, as well as change the relative proportion of hairs inside and outside it. To investigate this, we varied the bubble volume, $\hat{V}_b$, and compared the maximum adhesion force on both hydrophilic and hydrophobic substrates (Figure 7). The contribution of the bubble to the net adhesion force is small regardless of its volume, when compared to the whole pad. Further, opposite trends of adhesion is seen on the two substrates with changing $\hat{V}_b$.

From the previous section, we know that on the hydrophilic substrate, fluid bridges outside the bubble show poor adhesion due to the positive curvature of their meniscus. Thus, decreasing $\hat{V}_b$ decreases the adhesion force due to a larger proportion of hairs being

outside the bubble. In contrast, on the hydrophobic substrate, fluid bridges outside the bubble showed higher capillary forces, due to its low contact angle and high interfacial tension in water. Thus, adhesion force increases for a hydrophobic substrate as the bubble size decreases.

A smaller $\hat{V}_b$ resulted in increased, but small, attraction by the bubble on both types of substrates. For larger values of $\hat{V}_b$ however, the force trend for the whole pad mostly follows that of the bubble. This is because the bubble gets big enough to entrap all the hairs inside it. Thus, the force contribution due to the fluid bridges remain unchanged, and only the bubble's contribution drives the slight variation in the pad's adhesion at high $\hat{V}_b$. Once the bubble is small enough such that part of the fluid bridges start making contact in water, the force trend changes, with a steep decrease (increase) in adhesion force on hydrophilic (hydrophobic) substrate as the volume decreases.

3.5 Effect of hair diameter

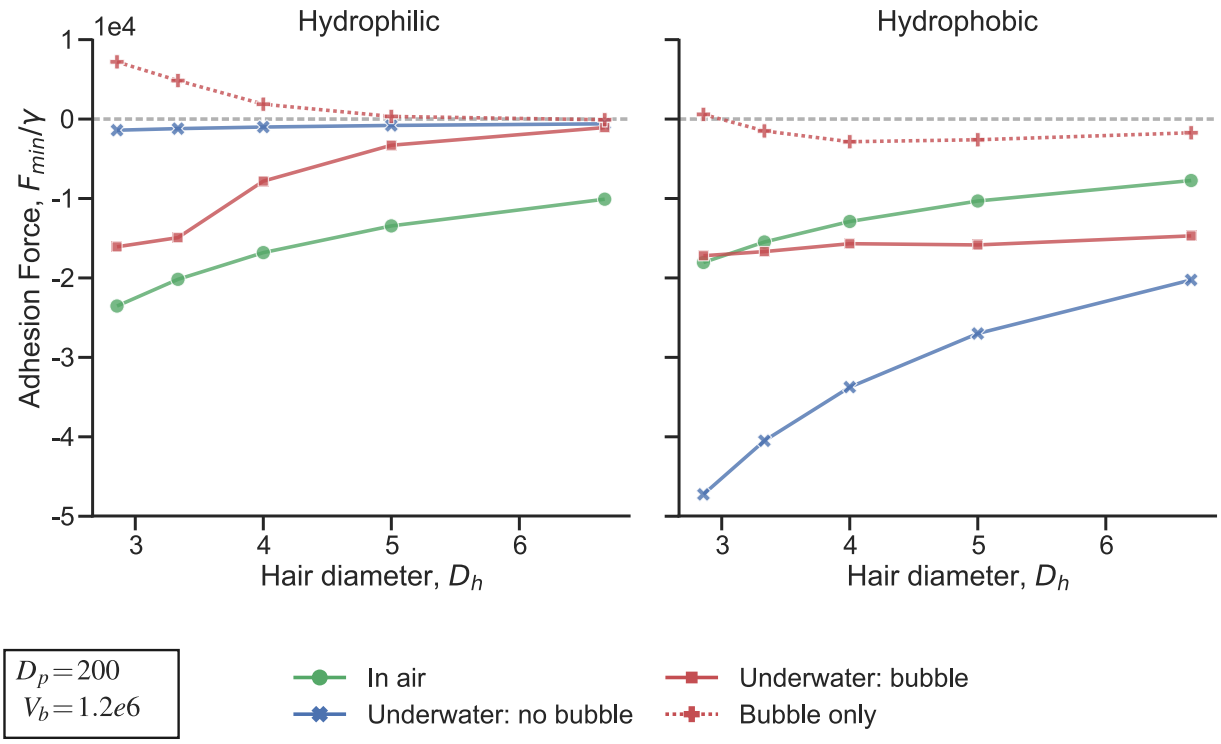

Figure 8: Normalised adhesion force of a hairy pad system on a hydrophilic and hydrophobic substrate as a function of hair diameter, D_h. Volume of each fluid bridge, V_f, scales relative to D_h based on the parameter $\phi_f = 2$. Adhesion forces are calculated from the minima of the respective force-distance curves, based on the capillary bridge model. A negative value represents attraction. The bubble's contribution to the net force for an *underwater: bubble* contact is denoted by plus symbols. Pad diameter and bubble volume are kept fixed. All lengths are scaled relative to D_p.

Hairs on a ladybug's pad terminate in various shapes like "discoidal" or "pointed". We studied this geometric effect on adhesion by changing the hair diameter, D_h (Figure 8). Here, the pad diameter, total hair contact area and bubble volume are constant since D_p, α and $\hat{V}_b$ are kept fixed. The adhesive fluid volume is again assumed to scale relative to the hair diameter ($\phi_f = 2$).

Adhesion force increases with decreasing D_h for both hydrophilic and hydrophobic substrates in all contact types. This is consistent with the "contact splitting" theory, which predicts higher adhesion when the contact is split into many small contact points[22]. Re-

ducing the hair diameter results in two competing effects: 1) capillary force due to a single fluid bridge decreases due to its smaller size and "self-similar" scaling assumption ($f \sim D_h$), which decreases the net force, and 2) total number of fluid bridges increases since the total hair contact area is assumed to be fixed ($N \sim 1/D_h^2$), which increases the net force. The second effect dominates, resulting in a higher adhesion force as D_h decreases.

Similar to the trend in Figure 5, contact *in air* shows the highest adhesion force on a hydrophilic substrate for the given range of hair diameters, while on a hydrophobic substrate, *underwater: no bubble* shows highest adhesion. *Underwater: bubble* contact shows intermediate adhesion between *in air* and *underwater: no bubble* contact types.

The bubble's contribution gets repulsive as hair diameter decreases for both substrates (Figure 8). Since the aspect ratio L/D_h is fixed (Table 3), decreasing the hair diameter also decreases its length. Since the bubble's volume is kept constant, it will then have a lesser space available to occupy between the pad and the substrate, This results in it bulging outwards near the pinned contact line on the top, causing repulsion.

4 Discussion

Our experiments demonstrate that the ladybug beetle can attach underwater to a hydrophobic substrate even without a bubble trapped around its hairs. A previous study[14] proposed that a bubble is necessary for underwater attachment in beetles. This is, however, only true for hydrophilic substrates, where a trapped bubble can facilitate underwater adhesion due to the hairs making contact in a de-wetted environment. For a hydrophobic substrate, the adhesion is similar regardless of whether the contact occurs in air or underwater conditions, with or without a trapped bubble. Our theoretical calculations further show that the bubble by itself has a negligible capillary contribution to the net underwater adhesion of the pad. Direct force measurement of a single similarly sized bubble making contact with a hydrophobic substrate shows a maximum adhesion less than 50 µN, which further validates that the

bubble's contribution is insignificant (A.5).

Predictions of the ladybug's adhesion from the capillary bridge model agree with our experimental results (Figure 2). In underwater conditions without a trapped bubble, adhesion to a hydrophobic substrate is significantly larger than to a hydrophilic substrate. This is explained by the different interfacial tension of the oil and contact angles with the substrates in air and underwater, which determines the capillary adhesive force in each case (Figure 6). However, the experiments don't show the predicted ~ 2.6 times increase in underwater adhesion relative to that in air on the hydrophobic PFOTS surface. This discrepancy could be due to our assumptions of the oily fluid's interfacial properties. If we choose γ_{fa}=30 mN/m and γ_{fw}=40 mN/m, the corresponding increase in adhesion will be ~ 1.7, closer to our experimental value of ~ 1. The resulting change in θ_{fa} and θ_{fw} will further decrease this number. Direct measurement of the fluid's interfacial properties is thus essential to better predict the insect's adhesion, and will be a subject of future studies. Further, due to surface inhomogeneities, not all the hairs might be able to completely drain the interfacial water layer, in order for the adhesive fluid to make a direct contact with the substrate. This can further reduce underwater adhesion, in comparison to our theoretical predictions which assumes a perfect contact.

In the model, we assume that all the hairs detach simultaneously to give a theoretical maximum achievable adhesion force. In our experiments, however, not all hairs make a perfect contact with the substrate despite our best efforts to align the pad with surface. Furthermore, during detachment, the pad typically peels off from its proximal to distal end rather than detach simultaneously. Our model also assumes the hairs to be of similar geometry, unlike the beetle's pad which has a distribution of flat or pointed tipped hairs. Thus, it's not surprising that the model overestimates the adhesion forces. The predictions are however in the same order of magnitude as experiments, and the qualitative trend is consistent for both hydrophilic and hydrophobic substrates in air and underwater.

Our study provides further validation that capillary forces govern insect adhesion and

van der Waals contribution, if any, must be negligible. Further, the capillary forces can even enable insect attachment underwater depending on the substrate chemistry. When underwater, without a trapped bubble, the pads adhere strongly to a hydrophobic substrate, but poorly to a hydrophilic substrate, even though it shows similarly strong adhesion to both substrates in air. This behaviour can only be explained by capillary forces and the wetting properties of the fluid. Our preliminary FDMS results further provides validation to our assumption that the adhesive fluid can form capillary bridges with the substrate in water, instead of getting washed away (Table 2).

The findings can also be extended to other animals relying on oily secretions for adhesion. Some ants, for example, show similar adhesion on hydrophobic substrates under wet and dry conditions[23], similar to what we see in a ladybug. Recent experiments on geckos revealed that they can attach well to fluoropolymer substrates underwater while they show little adhesion to the same substrate in air[24,25]. Geckos are thought to rely on van der Waals forces via dry contact with the substrate[10], although recent observations of phospholipid footprints left behind walking geckos[26] could change that picture. Since geckos adhere poorly to PTFE (surface energy $\sim$ 20 mN/m) one can speculate that the phospholipid material has a higher surface energy, and consequently makes a higher contact angle with PTFE in air. Let us assume the phosopholipid substance to be a fluid similar to oil with γ_{fa}= 30 mN/m and γ_{fw}= 42 mN/m such that its contact angle with PTFE is 80°. Equation 3 then gives us an underwater contact angle of 70° for the phospholipid fluid. Thus, on a PTFE surface, the capillary bridge model can predict a higher adhesion underwater than in air due to its lower contact angle and higher interfacial energy underwater. Based on similar assumptions, we predict the net adhesion force for the gecko on different substrates (Figure 9). The adhesion force predictions are in good qualitative agreement with the whole animal experimental shear force values reported for the gecko, with the trend of higher adhesion in air than underwater for glass, similar adhesion in air and underwater for PMMA/OTS-SAM and lower adhesion in air than underwater for PTFE. We, thus, propose that the underwater

experiments performed on geckos[24,25] indicate a capillary contribution to gecko adhesion. We suggest performing single seta adhesion force tests similar to Autumn et al.[10] using a hydrophilic and fluorinated probe in air and underwater conditions to validate the role of capillary contributions to gecko adhesion.

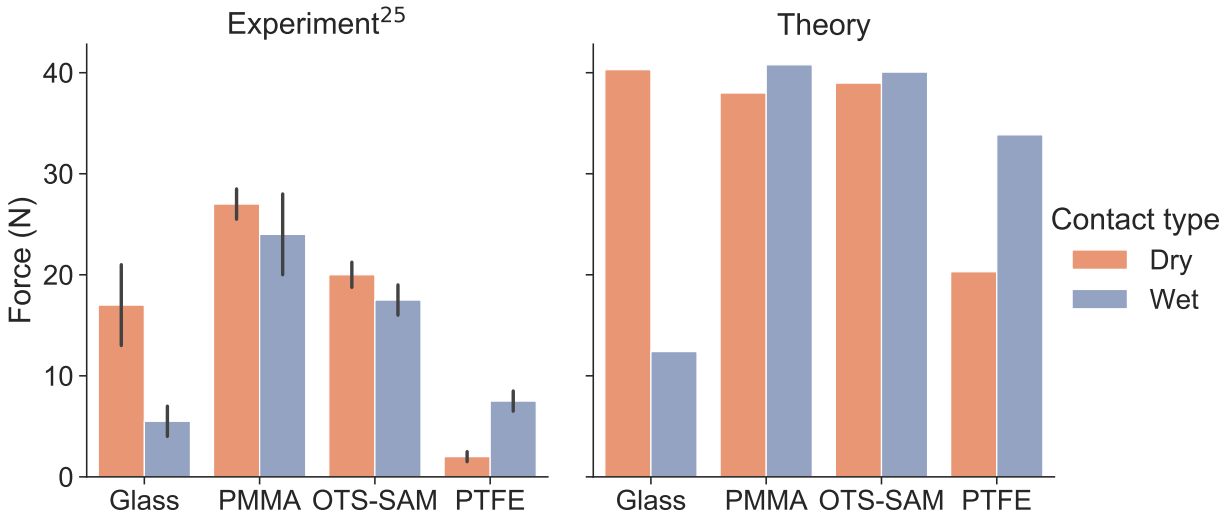

Figure 9: Whole animal adhesion force of geckos on various substrates. Experimental shear adhesion values are reproduced from Stark et al.[25]. Normal adhesion forces for each gecko toe are theoretically estimated from the capillary bridge model, with hair diameter = 400 nm, toe diameter = 4 mm, adhesive fluid volume = 4.19×10^{-3} fL and 10% hair coverage. "*Underwater: no bubble*" type contact is assumed for the "Wet" case. Net adhesion force is calculated by assuming 5 toes on each leg and 4 legs in total on a gecko. Interfacial tension of the phospholipid layer (PL) in air and water are assumed to be 30 mN/m and 42 mN/m respectively. PL contact angles with glass, PMMA, OTS-SAM and PTFE are assumed to be 6°, 10°, 20° and 80° respectively. The corresponding water contact angles are 50°, 85°, 94° and 97° respectively, as reported in Stark et al.[25].

We have so far limited our analysis to only smooth substrates. Of course insects have to cope with all kinds of surfaces including rough ones. Previous studies[27] have shown that substrate roughness is a more dominant parameter than substrate chemistry in controlling insect adhesion. Future work will explore how roughness can impact the net capillary force also in wet and submerged conditions. Our study thus can contribute to potential applications in the design of bio-inspired materials to achieve underwater adhesion via capillary bridges. Introduced bubbles can possibly be used to control underwater adhesion by chang-

ing the relative proportion of the arrays inside and outside the bubble. A suitable choice of adhesive fluid can be made tailored to the substrate and environment of application to achieve optimal adhesion performance.

5 Conclusions

Ladybug beetles rely primarily on their oily fluid secretion to adhere to surfaces in both air and underwater conditions. The beetles can attach underwater on a hydrophobic substrate even without a trapped air bubble within its hairy pad, although it loses this ability on a hydrophilic substrate. This is explained theoretically by the different contact angle and interfacial tension of the secreted fluid in air and underwater conditions. Further, the bubble itself has a negligible capillary contribution to the total force. The trapped bubble can promote adhesion only on a hydrophilic substrate by providing an air medium to the adhesive fluid bridges inside it. Oil wettability, thus, primarily controls the insect's adhesion in any given condition. A similar argument also explains previously reported underwater measurements in geckos[25], which highlights the possibility of capillary contributions to gecko adhesion. Future studies should characterise the fluid secretion's interfacial properties with a particular substrate to better understand the nature of the animal's adhesion.

6 Acknowledgement

We are grateful to Eduard Arzt and Renè Hensel for fruitful discussions. This work was funded by the *Deutsche Forschungsgemeinschaft* (Grant number: PI 1351/2-1).

A Appendix

A.1 Simulation method: Single capillary bridge

Capillary force due to a single adhesive fluid or bubble meniscus (termed "capillary bridge") is calculated by performing simulations in Surface Evolver[20], similar to the method described by De Souza et al.[21]. A simple cubic geometry, mimicking the capillary bridge, of constant volume, V, is defined as the initial condition with an interfacial tension, γ, with the surrounding medium. Interfacial tension of the capillary bridge with the substrate is given by $\gamma \cos\theta$, where θ is the corresponding contact angle inside the bridge. For the case of a bubble meniscus, θ is defined w.r.t. the surrounding water, since θ can also directly characterise the substrate wettability. The capillary bridge spans a gap distance d between the top face and the substrate. The boundary conditions are set corresponding to a pinned contact line of diameter D on the top face and constant interfacial tension with the substrate on the bottom. All lengths are normalised relative to length $s = (3V/4\pi)^{1/3}$. An appropriate geometry refinement routine is chosen to evolve the capillary bridge shape to its minimum energy state. The normalised total capillary force, $\hat{f} = f/\gamma s$, is the sum of the Laplace pressure and surface tension contributions , where:

$$f = f_{laplace} + f_{surface\,tension} = \Delta P_{laplace} A_{_{bottom}} + 2\pi R_{bottom} \gamma \sin\theta \tag{A.1}$$

Here, $\Delta P_{laplace}$ is the Laplace pressure of the equilibrium capillary bridge, A_{bottom} is the contact area of the capillary bridge with the substrate at bottom and R_{bottom} is the corresponding radius of contact, all obtained from the simulation output for the equilibrium surface.

The gap distance d is varied stepwise and the capillary force is calculated each time to obtain force-distance curves for a particular choice of D and θ.

A.2 Single capillary bridge: Effect of volume

Surface Evolver simulation results showing the effect of volume on the maximum capillary force of a single fluid bridge. Since the fluid is pinned at the top to the same diameter, D, a smaller volume would result in high interfacial curvatures, which increases the capillary force due to the negative Laplace pressure. In this case, small contact angles lead to a greater increase in adhesion.

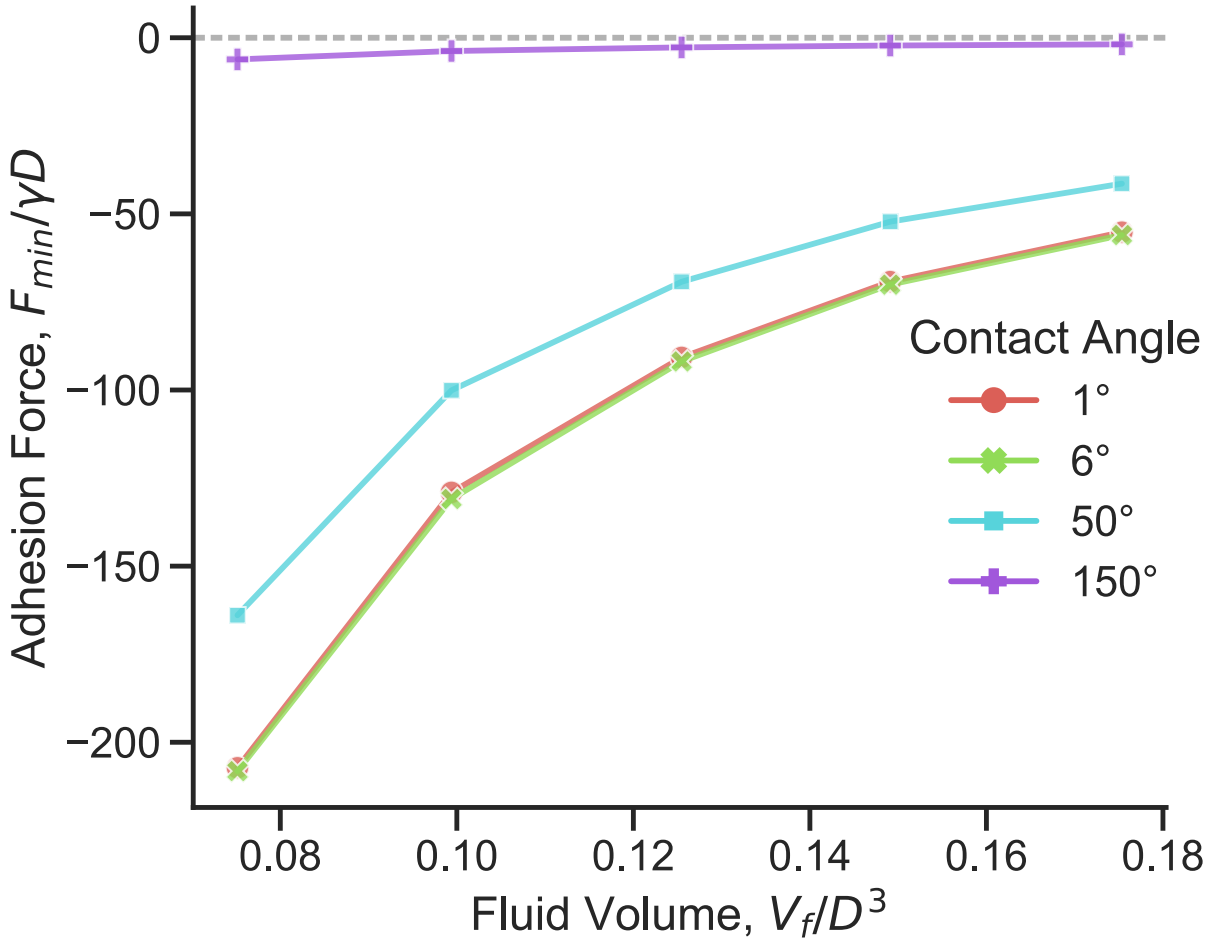

Figure A.1: Normalised maximum capillary force for a single bridge as a function of fluid volume

A.3 Capillary Bridge Model: Effect of hair diameter at constant fluid volume

Here, instead of scaling the fluid volume relative to the hair diameter, we now assume a fixed total fluid volume distributed equally among the N hairs. Total fluid volume, $V_{total} = NV_f = 2000$. Hair diameter is varied while keeping the total hair contact area constant. Length is in arbitrary units. Forces increase at a much smaller rate on decreasing diameter when compared to the case with self-similar scaling of fluid volume (Figure 8).

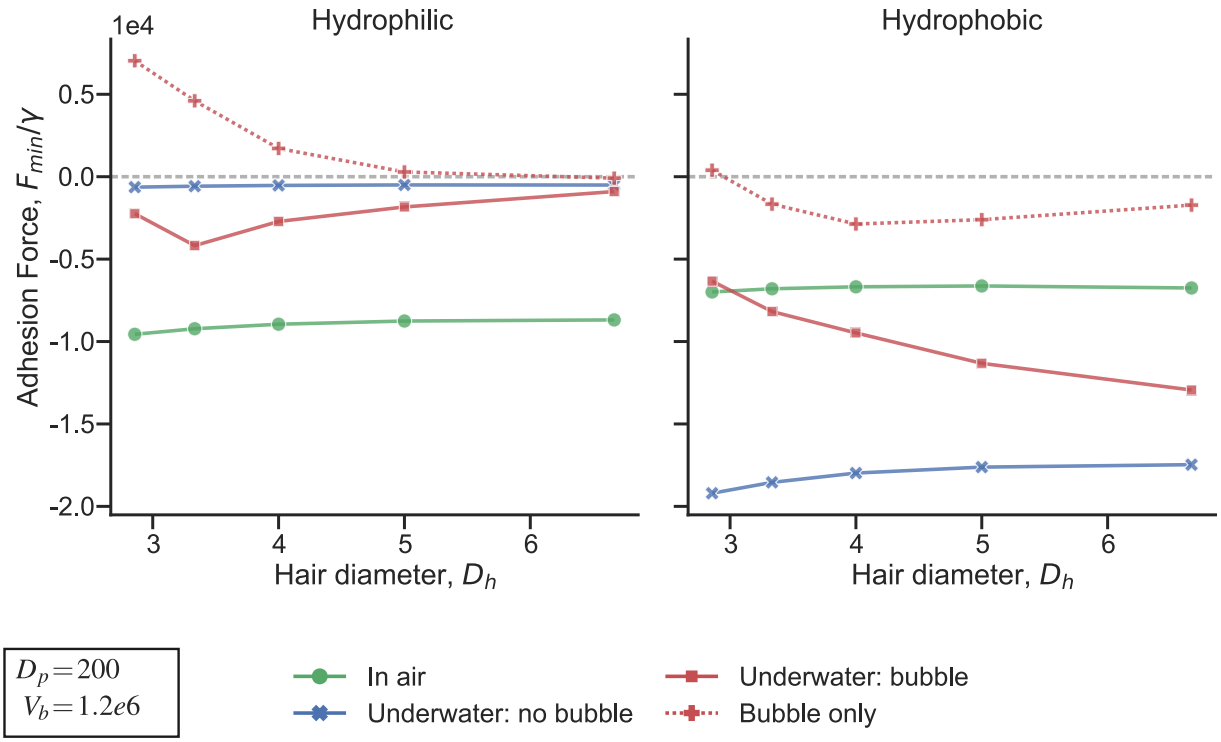

Figure A.2: Normalised adhesion force of hairy pad system on a hydrophilic and hydrophobic substrate as a function of hair diameter (D_h), calculated from the capillary bridge model. The total adhesive fluid volume is fixed to 2000. Adhesion forces are calculated from minima of the respective force-distance curves. Negative force value represents attraction. The bubble's contribution to the net force for an *underwater: bubble* contact is denoted by plus symbols. Bubble volume and pad diameter are kept fixed. All lengths are scaled relative to D_p.

A.4 Statistical comparison

Pairwise statistical comparison of single leg adhesion force measurements of the ladybug beetle (*Coccinella septempuctata*) for each contact type and substrate are shown (Table A.1). The uncorrected p-values and Common Language Effect Size (CLES) are obtained from post-hoc pair-wise Student t-test between A and B while keeping the third parameter fixed. p-values showing statistically significant difference between A and B are in boldface. The condition for statistical significance is based on the Bonferroni-corrected critical p-value of 0.008.

Table A.1

Fixed	A	B	p-value	CLES
In air	PFOTS	Glass	0.959	0.48
Underwater: bubble	PFOTS	Glass	0.011	0.96
Underwater: no bubble	PFOTS	Glass	$<$ **0.001**	1.0
PFOTS	In air	Underwater: bubble	0.897	0.48
PFOTS	In air	Underwater: no bubble	0.828	0.48
PFOTS	Underwater: bubble	Underwater: no bubble	0.721	0.44
Glass	In air	Underwater: bubble	**0.002**	1.0
Glass	In air	Underwater: no bubble	$<$ **0.001**	1.0
Glass	Underwater: bubble	Underwater: no bubble	0.07	0.84

A.5 Capillary force due to a bubble

Capillary force of a single bubble against a PFOTS surface are compared for two different volumes. The volumes correspond to the expected range in the case of the trapped bubble in a ladybug. Here, the bubble is pinned to a micropatterned PDMS substrate on the top. The maximum adhesion force of any of the bubble never exceeds 50 µN, significantly lower

than the beetle's underwater adhesion to the same substrate (> 400 µN). Thus, the bubble's contribution to adhesion in the "*underwater: bubble*" contact of a ladybug's pad should be negligible.

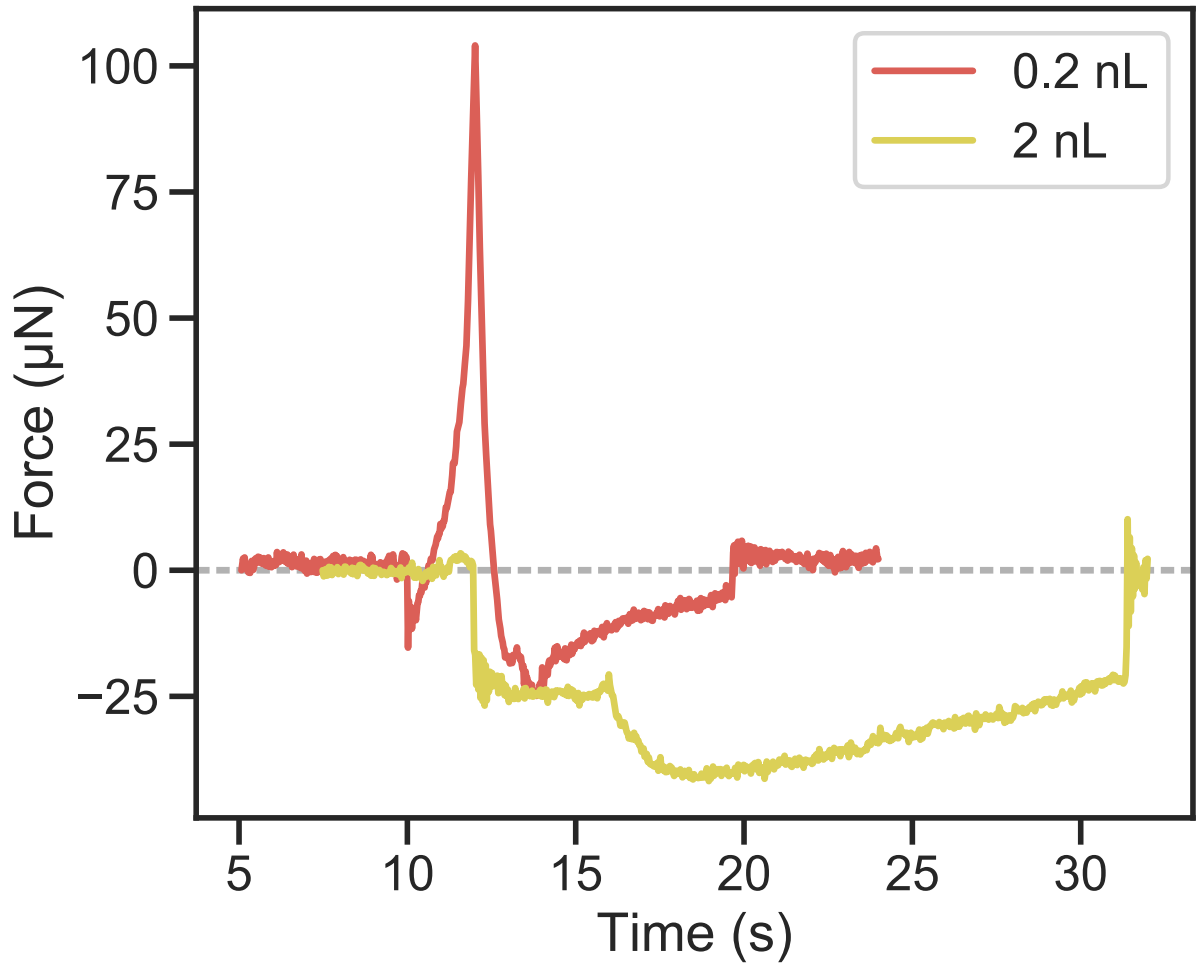

Figure A.3: Capillary force of the bubble

References

(1) Hooke, R. *Micrographia, or, Some physiological descriptions of minute bodies made by magnifying glasses : with observations and inquiries thereupon*; The Royal Society, 1665.

(2) Stork, N. E. Experimental Analysis of Adhesion of Chrysolina Polita (Chrysomelidae: Coleoptera) on a Variety of Surfaces. *The Journal of Experimental Biology* **1980**, *88*, 91.

(3) Gorb, S. N.; Beutel, R. G. Evolution of locomotory attachment pads of hexapods. *Naturwissenschaften* **2001**, *88*, 530–534.

(4) Coddington, J. A.; Levi, H. W. Systematics and evolution of spiders (Araneae). *Annual Review of Ecology and Systematics* **1991**, *22*, 565–592.

(5) Williams, E.; Peterson, J. Convergent and alternative disigns in the digital adhesive pads of scincid lizards. *Science* **1982**, *215*, 1509–1511.

(6) Federle, W. Why are so many adhesive pads hairy? *J Exp Biol* **2006**, *209*, 2611–21.

(7) Bullock, J. M.; Federle, W. Division of labour and sex differences between fibrillar, tarsal adhesive pads in beetles: effective elastic modulus and attachment performance. *J Exp Biol* **2009**, *212*, 1876–88.

(8) Bullock, J. M.; Federle, W. Beetle adhesive hairs differ in stiffness and stickiness: in vivo adhesion measurements on individual setae. *Naturwissenschaften* **2011**, *98*, 381–7.

(9) Dirks, J. H. Physical principles of fluid-mediated insect attachment - Shouldn't insects slip? *Beilstein J Nanotechnol* **2014**, *5*, 1160–6.

(10) Autumn, K.; Sitti, M.; Liang, Y. A.; Peattie, A. M.; Hansen, W. R.; Sponberg, S.; Kenny, T. W.; Fearing, R.; Israelachvili, J. N.; Full, R. J. Evidence for van der Waals adhesion in gecko setae. *Proceedings of the National Academy of Sciences* **2002**, *99*, 12252.

(11) Underwater attachment using hairs: the functioning of spatula and sucker setae from male diving beetles. *Journal of The Royal Society Interface* **2014**, *11*.

(12) Kang, V.; White, R. T.; Chen, S.; Federle, W. Extreme suction attachment performance from specialised insects living in mountain streams (Diptera: Blephariceridae). *bioRxiv* **2020**,

(13) Seymour, R. S.; Matthews, P. G. D. Physical gills in diving insects and spiders: theory and experiment. *Journal of Experimental Biology* **2013**, *216*, 164–170.

(14) Hosoda, N.; Gorb, S. N. Underwater locomotion in a terrestrial beetle: combination of surface de-wetting and capillary forces. *Proc Biol Sci* **2012**, *279*, 4236–42.

(15) Peisker, H.; Gorb, S. N. Evaporation dynamics of tarsal liquid footprints in flies (Calliphora vicina)and beetles (Coccinella septempunctata). *The Journal of Experimental Biology* **2012**, *215*, 1266–1271.

(16) Geiselhardt, S. F.; Geiselhardt, S.; Peschke, K. Comparison of tarsal and cuticular chemistry in the leaf beetle Gastrophysa viridula (Coleoptera: Chrysomelidae) and an evaluation of solid-phase microextraction and solvent extraction techniques. *Chemoecology* **2009**, *19*, 185.

(17) Attygalle, A. B.; Aneshansley, D. J.; Meinwald, J.; Eisner, T. Defense by foot adhesion in a chrysomelid beetle (Hemisphaerota cyanea): characterization of the adhesive oil. *Zoology* **2000**, *103*, 1–6.

(18) Ishii, S. Adhesion of a Leaf Feeding Ladybird Epilachna vigintioctomaculta (Coleoptera : Coccinellidae) on a Virtically Smooth Surface. *Applied Entomology and Zoology* **1987**, *22*, 222–228.

(19) Peattie, A. M.; Dirks, J.-H.; Henriques, S.; Federle, W. Arachnids secrete a fluid over their adhesive pads. *PloS one* **2011**, *6*, e20485–e20485.

(20) Brakke, K. A. The surface evolver. *Experiment. Math.* **1992**, *1*, 141–165.

(21) De Souza, E. J.; Brinkmann, M.; Mohrdieck, C.; Arzt, E. Enhancement of Capillary Forces by Multiple Liquid Bridges. *Langmuir* **2008**, *24*, 8813–8820.

(22) Arzt, E.; Gorb, S.; Spolenak, R. From micro to nano contacts in biological attachment devices. *Proc Natl Acad Sci U S A* **2003**, *100*, 10603–6.

(23) Stark, A. Y.; Yanoviak, S. P. Adhesion and running speed of a tropical arboreal ant (Cephalotes atratus) on wet substrates. *Royal Society open science* **2018**, *5*, 181540–181540.

(24) Stark, A. Y.; Dryden, D. M.; Olderman, J.; Peterson, K. A.; Niewiarowski, P. H.; French, R. H.; Dhinojwala, A. Adhesive interactions of geckos with wet and dry fluoropolymer substrates. *Journal of The Royal Society Interface* **2015**, *12*, 20150464.

(25) Stark, A. Y.; Badge, I.; Wucinich, N. A.; Sullivan, T. W.; Niewiarowski, P. H.; Dhinojwala, A. Surface wettability plays a significant role in gecko adhesion underwater. *Proc Natl Acad Sci U S A* **2013**, *110*, 6340–5.

(26) Hsu, P. Y.; Ge, L.; Li, X.; Stark, A. Y.; Wesdemiotis, C.; Niewiarowski, P. H.; Dhinojwala, A. Direct evidence of phospholipids in gecko footprints and spatula - substrate contact interface detected using surface-sensitive spectroscopy. *Journal of The Royal Society Interface* **2012**, *9*, 657–664.

(27) England, M. W.; Sato, T.; Yagihashi, M.; Hozumi, A.; Gorb, S. N.; Gorb, E. V. Surface roughness rather than surface chemistry essentially affects insect adhesion. *Beilstein journal of nanotechnology* **2016**, *7*, 1471–1479.